SECTOR-DELAYED-HOPF-TYPE MIXED-MODE OSCILLATIONS IN A PROTOTYPICAL THREE-TIME-SCALE MODEL

PETER DE MAESSCHALCK, EKATERINA KUTAFINA, AND NIKOLA POPOVIĆ

Abstract. We consider a three-dimensional three-time-scale system that was first proposed in [9] under the additional assumption that two singular perturbation parameters are present in the equations. While the presence of three scales was shown to give rise to canard-induced periodic mixed-mode oscillations (MMOs) [3] in the parameter regime studied in [9], we additionally observe mixed-mode patterns that display delayed-Hopf-type behaviour [12]. We present analytical and numerical evidence for the occurrence of stable periodic dynamics that realises both mechanisms, and we discuss the transition between them. To the best of our knowledge, the resulting mixed sector-delayed-Hopf-type MMO trajectories represent a novel class of mixed-mode dynamics in singularly perturbed systems of ordinary differential equations.

1. Introduction

In the present article, we consider a modification of a prototypical three-time-scale system of ordinary differential equations that was proposed in [9] as a canonical model for 'slow passage through a classical canard explosion' [10],

$$\varepsilon \dot{v} = -z + f_2 v^2 + f_3 v^3, \tag{1a}$$

$$\dot{z} = v - w, \tag{1b}$$

$$\dot{w} = \delta(\mu - g_1 z), \tag{1c}$$

where f_2 and g_1 are taken to be positive, while f_3 is negative, and the overdot denotes differentiation with respect to the 'slow' time variable τ. (For the numerical simulations presented in the article, we chose $f_2 = 1.5$, $g_1 = 0.5$, and $f_3 = -1$ throughout.) Moreover, all three of these parameters are assumed to be $\Theta(1)$, while both ε and δ are 'small' (singular) perturbation parameters, which implies the presence of one fast variable (v), one slow variable (z), and one 'super-slow' variable (w) in Equation (1). (Here and in the following, the notation $f(x) = \Theta(g(x))$ indicates that f is asymptotically bounded from above *and* from below by a multiple of $g(x)$ in the asymptotic limit as $(\varepsilon, \delta) \to (0, 0)$.) Finally, no *a priori* restriction is made on the order of the parameter μ; however, μ is not assumed to be asymptotically small in either ε or δ. The mathematical theory of singularly perturbed differential equations in which the dynamics varies on more than two distinct scales is not well-developed to date [8, 9]; nevertheless, such systems have attracted widespread interest in modelling applications, in particular in the life sciences. Recent examples include the mammalian dopaminergic neuron [7], intracellular calcium flow [5], and glycolytic oscillation [13], to name but a few.

Date: October 8, 2015.

2010 *Mathematics Subject Classification.* 34E10, 34E13, 34E15, 34E17, 37C27, 37G15, 92B05.

Key words and phrases. Mixed-mode oscillations; Delayed Hopf bifurcation; Canards; Neuronal modelling; Fast-slow dynamics; Singular perturbations.

The authors' research was supported by the Research Foundation Flanders (FWO) under grant number G.0939.10N. Moreover, E. K. acknowledges support from the Polish Ministry of Science and Higher Education. Finally, the authors thank three anonymous reviewers whose comments and suggestions greatly improved the original manuscript.

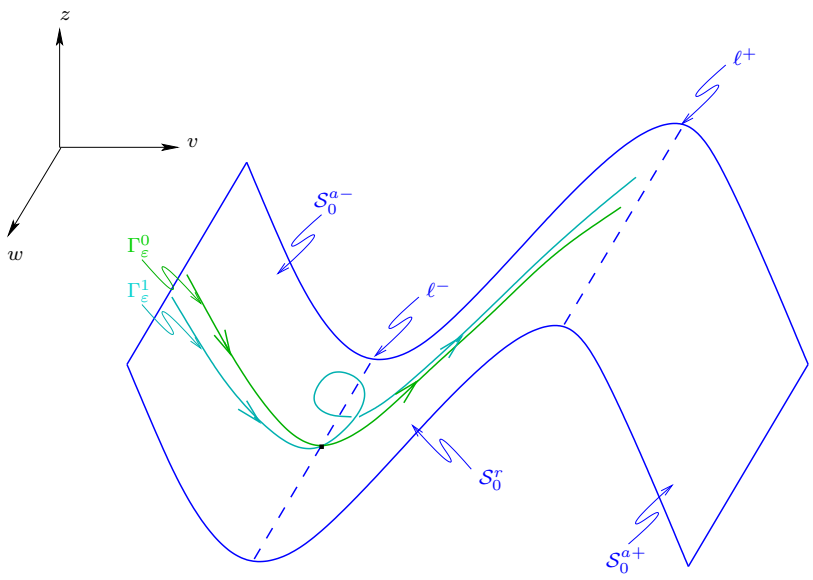

FIGURE 1. Fast-slow geometry of (1). The sheets $\mathcal{S}_0^{a-}$, $\mathcal{S}_0^r$, and $\mathcal{S}_0^{a+}$ of $\mathcal{S}_0$ are separated by fold lines $\ell^\mp$ at which normal hyperbolicity is lost; the strong canard Γ_ε^0 (solid green) and the first secondary canard Γ_ε^1 (solid turquoise) are superimposed.

While Equation (1) possesses an underlying three-time-scale structure, it can also be interpreted as a standard fast-slow system with one singular perturbation parameter ε for which a two-dimensional critical manifold $\mathcal{S}_0$ is obtained by taking $\varepsilon = 0$: $\{z = f(v)\}$, with $f(v) = f_2v^2 + f_3v^3$. Under the above assumptions on f_j $(j = 2, 3)$, the manifold $\mathcal{S}_0$ is cubic-shaped, with two attracting sheets $\mathcal{S}_0^{a-}$ and $\mathcal{S}_0^{a+}$ and one repelling sheet $\mathcal{S}_0^r$ in between. The three sheets are separated by two fold lines ℓ^- and ℓ^+, which are determined by the additional condition that $f'(v) = 0$; the resulting geometry is illustrated schematically in Figure 1. Fenichel's geometric singular perturbation theory [4, 6] guarantees that, for ε positive and small, $\mathcal{S}_0^{a-}$, $\mathcal{S}_0^r$, and $\mathcal{S}_0^{a+}$ perturb to corresponding sheets $\mathcal{S}_\varepsilon^{a-}$, $\mathcal{S}_\varepsilon^r$, and S_ε^{a+} of a slow manifold $\mathcal{S}_\varepsilon$, provided one stays away from the fold lines $\ell^\pm$ at which there is a loss of normal hyperbolicity in (1). (We may use the same notation as in [9, Section 2.1] here, *i.e.*, we need not interpret Equation (1) as a two-parameter singular perturbation problem, as we will assume an interdependence between ε and δ in the following; in particular, we will consider $\delta = \Theta(\sqrt{\varepsilon})$.)

The case where $\delta = \varepsilon$ in Equation (1) was studied in detail in [9]; specifically, the existence and stability of mixed-mode trajectories was proven which consist of both SAOs (small-amplitude oscillations) and LAOs (large-amplitude oscillations) in alternation. The resulting mixed-mode oscillations (MMOs) were described in terms of their so-called Farey sequences $L_1^{s_1}L_2^{s_2}\ldots$, which encode the signatures of admissible oscillatory patterns therein. (Thus, the segment $L_j^{s_j}$ represents L_j LAOs, followed by s_j SAOs, in the mixed-mode trajectory.) Moreover, μ was identified as the natural bifurcation parameter for unfolding the mixed-mode dynamics of Equation (1), in the sense that a cascade of MMOs with varying Farey sequences is observed as μ is varied. Finally, asymptotic estimates were given for the relevant μ-intervals that correspond to the Farey signatures realised in that unfolding.

Most importantly for our purposes, the occurrence of mixed-mode dynamics in Equation (1) was shown to be due to the presence of a 'folded saddle-node of type II' at the origin provided μ is sufficiently small; the former is defined as a saddle-node equilibrium of (1) on ℓ^- which, additionally, constitutes an equilibrium for an appropriately defined desingularisation of (1) about

ℓ^-. (The reader is referred to [3, 9] for details and references on the theory of canard-induced MMOs in general, and on the terminology used here in particular. For completeness, we emphasise that, for μ 'large', the corresponding equilibrium will be a 'folded saddle-node of type I' [11].) For ε sufficiently small, the super-slow variable w was interpreted as a slowly varying parameter in [9]. The system was then seen to undergo slow passage through a classical 'canard explosion' in the planar (v, z)-subsystem in (1). The resulting near-integrable structure close to the origin in (v, z, w)-space allowed for a precise asymptotic description of the SAO dynamics there. Specifically, the latter was shown to be induced by the passage of trajectories through a sequence of 'sectors of rotation', which can be visualised loosely as a partition of the w-axis close to the 'strong canard' Γ_ε^0 in the system, cf. Figure 1, with each SAO corresponding to one such sector. As is common in the context of fast-slow systems of the standard form in (1), the LAO component of the resulting mixed-mode trajectories then arises due to a global return mechanism that is typical of relaxation oscillators with cubic-shaped slow manifold. In sum, the mixed-mode dynamics of Equation (1) hence originates from a subtle interplay between a local passage through a neighbourhood of the fold line ℓ^- in (1) and the global return mechanism which re-injects the flow into that neighbourhood after relaxation.

Under the key restriction that $w = \Theta(\varepsilon)$ in Equation (1), it was shown in [9] that the flow will always return sufficiently close to the so-called strong canard, thus resulting in periodic, 'sector-type' mixed-mode dynamics. In the parameter regime considered in [9], with $\delta = \varepsilon$, that restriction is generically met. However, when $\delta > \varepsilon$, which is the scenario studied in this article, the global relaxation mechanism may be sufficiently strong to allow for a return further away from the strong canard. In that case, a different type of mixed-mode dynamics is observed, which will be termed the 'delayed-Hopf type' in the following.

Delayed passage through a Hopf bifurcation in a neighbourhood of a folded saddle-node of type II was investigated in [11]. Specifically, a canonical system of the form

$$\dot{x} = y - (\mu + 1)z + \mathcal{O}[x, \varepsilon, (y + z)^2], \tag{2a}$$

$$\dot{y} = \frac{1}{2}\mu + a_1\, y + a_2\, z + \mathcal{O}[x, \varepsilon, (y + z)^2], \tag{2b}$$

$$\varepsilon\dot{z} = x + z^2 + \mathcal{O}[z^3, xz^2, xyz, \varepsilon(x + y + z), \varepsilon^2] \tag{2c}$$

was studied under the condition that $a_1 + a_2 < 0$. (The condition guarantees, in particular, that (2) admits a stable node on $\mathcal{S}_0^{a-}$ for $\mu > 0$ and a saddle on $\mathcal{S}_0^r$ for $\mu < 0$ sufficiently small; the reader is referred to [11] for details.) It was shown that the local behaviour of Equation (2) is not determined by passage past a fold anymore, but, rather, past a curve that can be interpreted as a one-dimensional ε-family of critical manifolds after an appropriate rescaling; cf. Section 2 below for a more complete discussion. Since the amplitude of SAOs generated in a delayed passage through a Hopf bifurcation is typically so small that their number cannot be detected, we will denote such segments with the signature L^d, in which L LAOs are followed by some unspecified number d of SAOs.

Even for $\delta = \varepsilon$ in Equation (1), we may observe the existence of delayed-Hopf-type mixed-mode segments if the system is initially forced away from the strong canard. In Figure 2, we present one example of such a segment that was obtained with $\varepsilon = 0.01 = \delta$, $\mu = 0.02$, and the initial condition $(v_0, z_0, w_0) = (0.1, 0, 0)$. The signature 1^d1^8 is seen in the resulting time series of v, whereby a delayed-Hopf-type segment (dashed red) is followed by one of sector type (solid blue); cf. Figure 2(a). Figure 2(b) illustrates the corresponding orbit in phase space: the initial value of w is far enough from the strong canard to allow for delayed passage through a Hopf bifurcation, shown in red; upon relaxation, the orbit returns sufficiently close to the strong canard to be attracted to the stable (sector-type) canard-induced MMO depicted in blue, as predicted in [9].

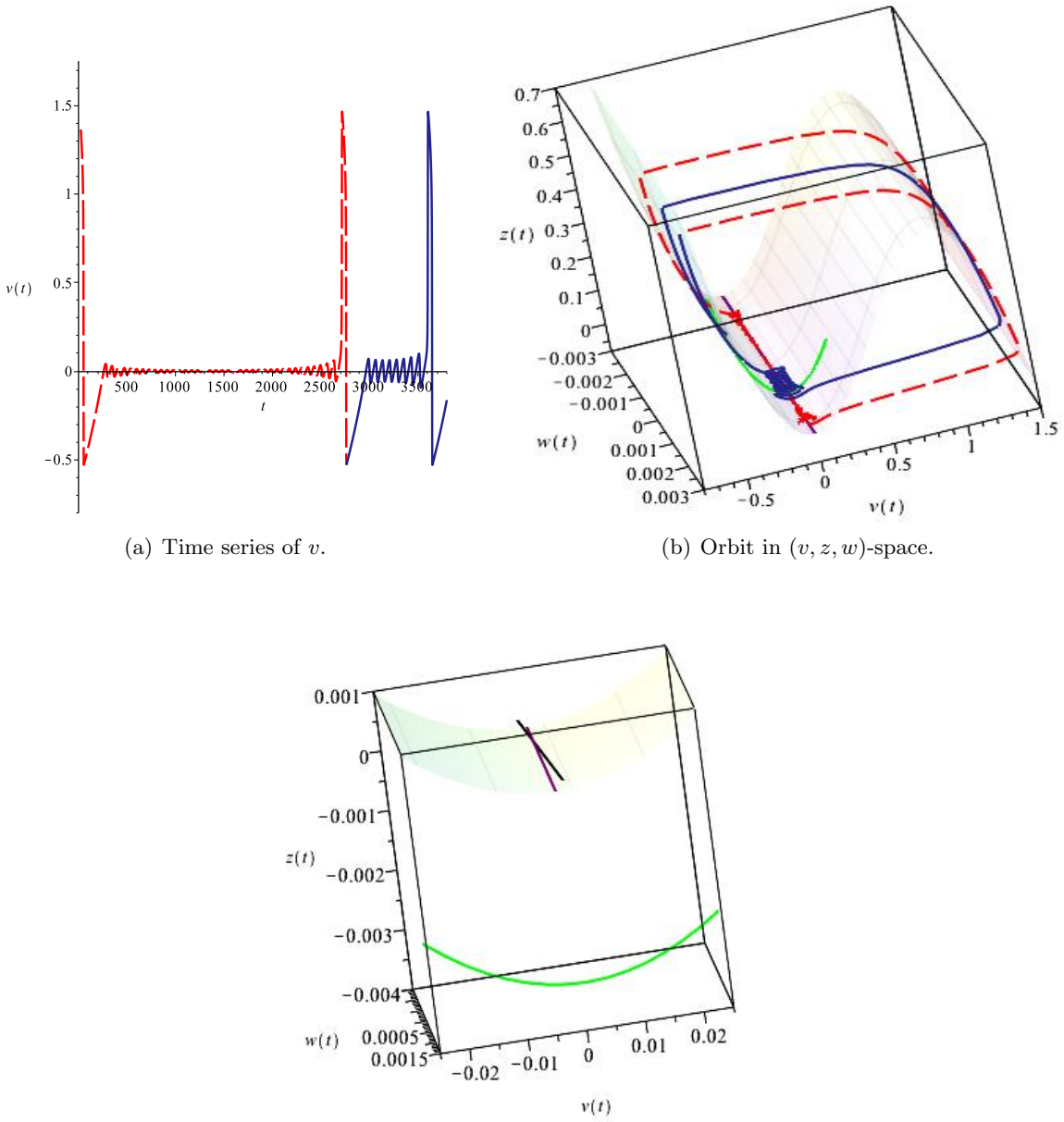

(a) Time series of v.

(b) Orbit in (v, z, w)-space.

(c) Zoom onto fold region.

FIGURE 2. Mixed sector-delayed-Hopf-type pattern for $\delta = \varepsilon$ in (1) (1^d1^8; $\varepsilon = 0.01 = \delta$, $\mu = 0.02$). For reference, the strong canard Γ_ε^0 (solid green), the fold line ℓ^- (solid purple), and the critical manifold $\mathcal{S}_0$ (shaded) are included in panel 2(b). The zoom onto the fold region in panel 2(c) reveals the manifold $\mathcal{M}_\varepsilon$ (solid black), which is indistinguishable from ℓ^- on the scale of 2(b).

Remark 1. *Throughout, numerical simulations have been performed in* MAPLE *on the basis of the fast system that is obtained from Equation* (1) *after introduction of the rescaled time variable* $t = \frac{\tau}{\varepsilon}$. □

While Equation (1) can be transformed into (2) locally about its folded-saddle node at the origin, the results of [11] do not hold for the resulting system, as $a_1 + a_2 = 0$ in our case. (That degeneracy underlies, in particular, the three-time-scale structure of (1), whereby the passage of an equilibrium along $\mathcal{S}_0$ in Equation (2) is replaced with a slow drift in the w-variable in (1).) However, as will become clear in the following, standard results on delayed passage through a Hopf bifurcation [12] can be applied to describe delay effects for $\delta > \varepsilon$ in (1) that are very similar to those found in [11]. Here, we will investigate some of the mixed-mode dynamics which emerges in Equation (1) in that scenario via a combination of non-rigorous asymptotics and numerical heuristics. In particular, by changing the hierarchy of scales to a sufficient degree, we will construct periodic orbits of 'mixed sector-delayed-Hopf type' for (1) in which segments of sector type alternate with those of delayed-Hopf type, and which thus realise both mechanisms. In light of the above discussion, the presence of both sector-type and delayed-Hopf-type dynamics in Equation (1) is hence due to different unfoldings of a higher-codimension singularity – as either slow passage through a canard explosion [9] or dynamic Hopf bifurcation in the presence of an equilibrium [11]. The resulting MMOs possibly represent a novel type of stable periodic solution trajectories to three-time-scale systems of the type in (1).

This article is organised as follows. In Section 2, we discuss the local dynamics of Equation (1), both in the sector-type and the delayed-Hopf-type regimes: we derive a local ('zoomed') formulation for (1) in which the potential for the two types of dynamics becomes apparent, and we provide a brief analysis of both regimes. In Section 3, we consider the global dynamics of Equation (1): following [9], we approximate the global return mechanism to leading order, and we conceptualise a reduced (one-dimensional) Poincaré map that is based on the discussion in the preceding section. In Section 4, we provide numerical evidence for the existence of stable periodic MMO trajectories of mixed sector-delayed-Hopf type in the regime where $\delta = \Theta(\sqrt{\varepsilon})$, and we explicitly perform a simplistic asymptotic reduction for the Poincaré map corresponding to these trajectories. Finally, in Section 5, we discuss the results of our study, and we provide pointers for future research.

2. Local dynamics

In this section, we describe the dynamics of Equation (1) in a neighbourhood of the origin in (v, z, w)-space, where we now assume that $\delta > \varepsilon$. We motivate the existence of solution trajectories in that scenario which incorporate both sector-type and delayed-Hopf-type segments; then, we perform a local analysis of (3) to show how these two types of segment can be constructed. While much of the asymptotics derived in [9] for the specific case of $\delta = \varepsilon$ in Equation (1) is not valid anymore, the general picture is mostly preserved: near the origin, the flow of (1) is still described by a near-integrable system; however, different scalings for w are now required in order to distinguish between sector-type and delayed-Hopf-type dynamics.

2.1. Motivation.

Following the procedure in [9, Section 2.2], we perform a 'zoom' onto a neighbourhood of the origin in (1), making the change of coordinates

$$v = \sqrt{\varepsilon}\bar{v}, \quad z = \varepsilon\bar{z}, \quad w = \sqrt{\varepsilon}\bar{w}, \quad \text{and} \quad t = \sqrt{\varepsilon}\bar{t};$$

thus, we obtain the following system of equations:

$$\dot{\bar{v}} = -\bar{z} + f_2\bar{v}^2 + \sqrt{\varepsilon}f_3\bar{v}^3, \tag{3a}$$

$$\dot{\bar{z}} = \bar{v} - \bar{w}, \tag{3b}$$

$$\dot{\bar{w}} = \delta(\mu - \varepsilon g_1\bar{z}). \tag{3c}$$

(Here, the overdot now denotes differentiation with respect to the rescaled time $\bar{t}$.) The first two equations in (3) can be interpreted as a planar system with parameter $\bar{w}$: for $\bar{w}$ fixed, there is a

stationary point at $(\bar{v},\bar{z}) = (\bar{w}, f_2\bar{w}^2 + \sqrt{\varepsilon} f_3 \bar{w}^3)$ in the $(\bar{v},\bar{z})$-subsystem in (3); the corresponding eigenvalues are easily calculated as

$$\lambda_\pm = \Big(f_2 + \frac{3}{2}\sqrt{\varepsilon} f_3 \bar{w}\Big)\bar{w} \pm \sqrt{\Big(f_2 + \frac{3}{2}\sqrt{\varepsilon} f_3 \bar{w}\Big)^2 \bar{w}^2 - 1}. \tag{4}$$

Since we assume f_2 to be positive and $\Theta(1)$, while an *a posteriori* estimate as in [9] shows that $\bar{w}$ is certainly $\mathcal{O}(1)$, we find a stable focus for $\bar{w} < 0$ and an unstable focus for $\bar{w} > 0$, with a Hopf bifurcation occurring at $\bar{w} = 0$ provided $\varepsilon \in [0, \varepsilon_0]$, with $\varepsilon_0 > 0$ sufficiently small; in particular, for $\varepsilon = 0 = \bar{w}$, the $(\bar{v},\bar{z})$-subsystem in Equation (3) becomes integrable.

When $\bar{w}$ is non-zero, but small, (3) can hence be interpreted as a perturbation off an integrable system, as was done in [9]. Alternatively, one may note that, for $\bar{w}$ in some fixed interval and ε sufficiently small, Equation (3) admits a one-dimensional ε-family of critical manifolds

$$\mathcal{M}_\varepsilon := \big\{(\bar{v},\bar{z},\bar{w}) \,\big|\, \bar{v} = \bar{w}, \bar{z} = f_2\bar{w}^2 + \sqrt{\varepsilon} f_3 \bar{w}^3, \bar{w} \in [-\bar{w}_0, \bar{w}_0]\big\}, \tag{5}$$

where $\bar{w}_0 > 0$ is suitably chosen. Hence, Equation (3) represents an example of a dynamic Hopf bifurcation along a slow manifold [12]. Intuitively speaking, the following picture emerges; see again Figure 2 for an illustration: for sufficiently small initial values of $\bar{w}$, the analysis in [9] applies, *i.e.*, the corresponding orbit (solid blue) passes through a number of 'sectors of rotation' before being ejected from the fold region, as shown in Figure 2(b). If, on the other hand, $\bar{w}$ is sufficiently large in absolute value for the orbit to be attracted to $\mathcal{M}_\varepsilon$ before it reaches the fold, one observes delayed-Hopf-type behaviour [12]: the orbit (dashed red) crosses the fold region following $\mathcal{M}_\varepsilon$ and is then repelled away, as illustrated in Figure 2(b). (For reference, the fold curve ℓ^- – which is given by the w-axis in our case – is superimposed in purple; since ℓ^- is indistinguishable from $\mathcal{M}_\varepsilon$ on the scale of Figure 2(b), a zoom onto the fold region is shown in Figure 2(c).) In both cases, the corresponding orbit undergoes a number of SAOs during its local passage, the amplitude of which will be clearly discernible in the sector regime, whereas it may be indiscernible in the delayed-Hopf regime; recall Figure 2(a).

In combination with an appropriately defined global return mechanism – which is determined by Equation (1c), cf. Section 3.1 below – it hence seems plausible that time-series of mixed sector-delayed-Hopf type can emerge. The precise nature of the resulting dynamics will depend, in a subtle fashion, on the interplay between the local and the global dynamics of Equation (3) and, in particular, on the relative magnitudes of the parameters ε, δ, and μ. While a fully rigorous analysis is beyond the scope of the present study, some intuition is provided in the following subsection.

2.2. **Analysis.** In this subsection, we analyse in turn the local dynamics of Equation (1) – *i.e.*, of the rescaled Equation (3) – in the sector-type and the delayed-Hopf-type regimes. The aim of our analysis is the derivation of a reduced, one-dimensional Poincaré map for (1) that will be a function of the super-slow variable w only, as in [9]. In the following, we may hence restrict ourselves to approximating the evolution of the variable $\bar{w}$ under the flow of Equation (3) in the two regimes.

2.2.1. *Sector-type dynamics.* We recall Equation (3), as well as the fact that the only difference to the corresponding system in [9, Section 2.2] is due to ε having been replaced with δ in (3c). Moreover, and again as in [9], we introduce the section $\Delta : \{v = 0\}$ and its rescaled counterpart $\overline{\Delta} : \{\bar{v} = 0\}$, as well as the 'half-section' $\overline{\Delta}_- := \overline{\Delta} \cap \{\bar{z} < 0\}$. Finally, we note that the singular system which is obtained from (3) for $\varepsilon = 0 = \delta$ agrees with Equation (2.4) in [9]:

$$\dot{\bar{v}} = -\bar{z} + f_2\bar{v}^2, \tag{6a}$$

$$\dot{\bar{z}} = \bar{v} - \bar{w}, \tag{6b}$$

$$\dot{\bar{w}} = 0. \tag{6c}$$

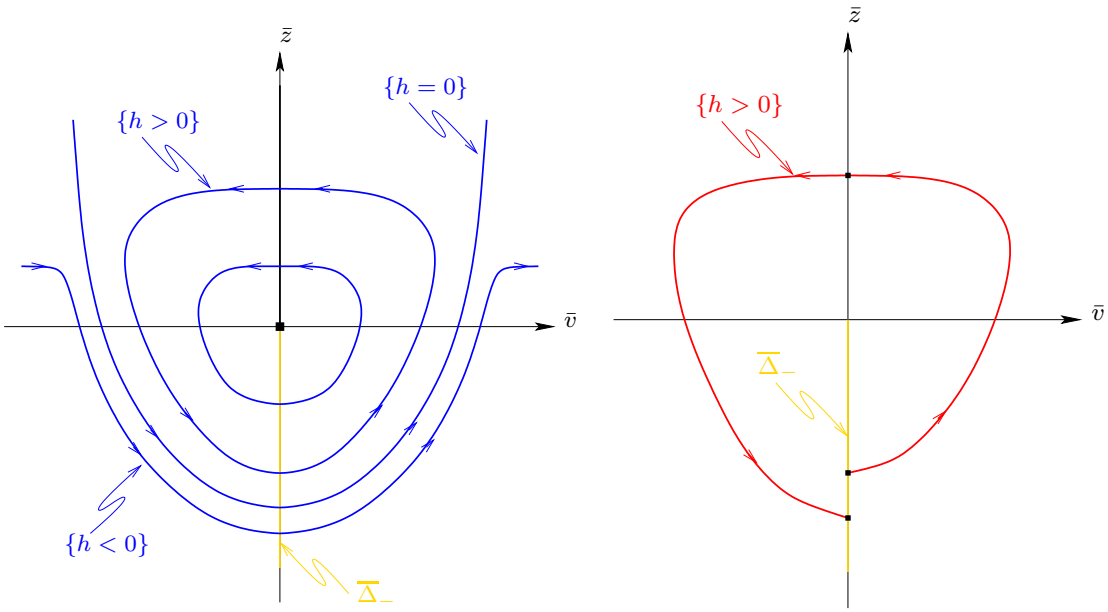

(a) $\varepsilon = 0 = \delta$. (b) $0 < \varepsilon < \delta$.

FIGURE 3. Near-integrable geometry of (3). Panel 3(a) illustrates the level curves of the constant of motion H with varying h; in panel 3(b), the perturbation off one such curve is sketched for $h > 0$.

For $\bar{w} = 0$, Equation (6) admits the constant of motion $H(\bar{v}, \bar{z}) = \frac{1}{2}\mathrm{e}^{-2f_2\bar{z}}\big(-\bar{v}^2 + \frac{\bar{z}}{f_2} + \frac{1}{2f_2^2}\big)$ [9, Equation (2.5)]; the corresponding level curves, which are defined by $H(\bar{v}, \bar{z}) = h$, are closed when $h > 0$ and open when $h < 0$. (The curve obtained for $h = 0$ is special, as it separates these two families of curves; see Figure 3(a) for an illustration.) As indicated above, we are only interested in describing the $\bar{w}$-component of the transition map $\overline{\Pi}^{\mathrm{sec}} : \overline{\Delta}_- \to \overline{\Delta}_-$ that is induced by the flow of Equation (3):

Lemma 1. *To leading order in ε and δ, the map $\Pi^{\mathrm{sec}} : \Delta_- \to \Delta_-$ is given by*

$$\Pi^{\mathrm{sec}}(w) = w + 2\sqrt{2}\mu\delta\sqrt{\varepsilon}\sqrt{-\ln\varepsilon} + \mathcal{O}(\delta\sqrt{\varepsilon}) \quad \textit{for } w = \Theta(\varepsilon), \tag{7}$$

provided $\varepsilon \in [0, \varepsilon_0]$.

Proof. Following the proof of [9, Proposition 2.2], we approximate (3c) with the truncated equation $\dot{\bar{w}} = \delta\mu$, which we then integrate to find $\overline{\Pi}^{\mathrm{sec}}(\bar{w}) = \bar{w} + \delta\mu T^h(\bar{w}) + \mathcal{O}(\delta^2)$; here, $T^h(\bar{w})$ denotes the return time of solutions to $\overline{\Delta}_-$, as illustrated in Figure 3(b). Since that time is determined by perturbing off the integrable dynamics of (6), it follows as in [9] that $T^h(\bar{w}) \sim T^h(0) = 2T^h$, where $T^h = \sqrt{2}(-\ln h)^{\frac{1}{2}} + \mathcal{O}(1)$ [9, Lemma A.2]. (Here and in the following, the tilde denotes the leading-order asymptotic approximation of some given expression in the singular perturbation parameters ε or δ, as appropriate.) Practically speaking, it suffices to assume that $h = \Theta(\varepsilon)$, as was also done in [9, Section 3.3]; in terms of the original w-variable, one then obtains the leading-order approximation for Π^{sec} in Equation (7), which is valid as long as $w = \Theta(\varepsilon)$ holds, in accordance with the scaling assumed in the present sector-type regime. □

We note that the above *a posteriori* estimate $\bar{w} = \mathcal{O}(1)$ implies $w = \mathcal{O}(\sqrt{\varepsilon})$, which is weaker than the condition imposed in Lemma 1. In the subsequent subsection, we will consider a complementary regime, with $\bar{w} = \Theta(\varepsilon^\alpha)$ for $0 < \alpha < \frac{1}{2}$.

Remark 2. *For completeness, we remark that to any* $0 \leq h \leq (4f_2^2)^{-1}$*, there corresponds precisely one value of* $\bar{z}$ *in* $\overline{\Delta}_-$ [9, Proposition 2.1]*. Hence, the* $\bar{z}$*-component of* $\overline{\Pi}^{\text{sec}}$ *can be described in terms of* h *by perturbation off the singular system, Equation* (6)*, as was also done in* [9, Section 2.2]. □

Finally, Figure 3 illustrates the formation of sector-type SAO dynamics in Equation (3): given a fixed, positive value of h, one return to $\overline{\Delta}_-$ under the corresponding flow represents one such oscillation; recall Figure 3(b). For ε and δ sufficiently small, the resulting SAO is close to the singular 'template' that is obtained from the level curve of H with that same h-value when $\varepsilon = 0 = \delta$, as shown in Figure 3(a).

2.2.2. *Delayed-Hopf-type dynamics.* Throughout this subsection, we will disregard any relation between δ and ε in Equation (3), considering δ as the singular parameter for arbitrary $\varepsilon \in [0, \varepsilon_0]$, with ε_0 sufficiently small. (Parameter regimes where $\delta = \Theta(\varepsilon)$ or $\delta = \Theta(\sqrt{\varepsilon})$ are hence sub-scenarios of the scenario studied here.) We will again restrict our analysis to a region in phase space where $\bar{w} = \mathcal{O}(1)$; more specifically, we will assume $\bar{w} = \Theta(\varepsilon^\alpha)$ for some $0 < \alpha < \frac{1}{2}$. That restriction will allow us to describe the local return from the section Δ_- to itself in a complementary w-regime to the one considered in the previous subsection.

For $\delta = 0$ and $\varepsilon \in [0, \varepsilon_0]$, Equation (3) reduces to

$$\dot{\bar{v}} = -\bar{z} + f_2\bar{v}^2 + \sqrt{\varepsilon} f_3 \bar{v}^3, \tag{8a}$$

$$\dot{\bar{z}} = \bar{v} - \bar{w}, \tag{8b}$$

$$\dot{\bar{w}} = 0, \tag{8c}$$

with a curve of singularities given by the manifold $\mathcal{M}_\varepsilon$ about which the linearisation of the vector field has the eigenvalues $\lambda_\pm = f_2\bar{w} \pm \sqrt{(f_2\bar{w})^2 - 1} + \mathcal{O}(1)$ for $\varepsilon \to 0$; recall Equations (4) and (5).

Under the restriction on $\bar{w}$ imposed in the present subsection, these two eigenvalues are complex conjugates, which implies that all points on $\mathcal{M}_\varepsilon$ are foci (or centres). More importantly, we thus avoid the region in phase space where transitions from focus to node or vice versa may arise. (That more general, and far more delicate, case has been studied in detail in [1, 11].)

At $\bar{w} = 0$ in (8), a Hopf bifurcation occurs, with $\bar{w}$ as the bifurcation parameter; hence, for $\delta > 0$ small, Equation (3) experiences slow passage through a Hopf bifurcation during which one can expect to encounter the phenomenon of bifurcation delay. While orbits are drifting along $\mathcal{M}_\varepsilon$, they are rotating with some rotation speed that is $\Theta(1)$. Thus, a drift of magnitude $\Delta\overline{W}$ in the $\bar{w}$-direction yields $\Delta\overline{W} \cdot \Theta(\delta^{-1})$ rotations. Since our focus is on a window in phase space that is of width $\Theta(\varepsilon^\alpha)$ in $\bar{w}$, the corresponding orbits will undergo $\Theta(\varepsilon^\alpha\delta^{-1})$ rotations.

Hence, we conclude that the true singular perturbation parameter in that window is $\frac{\delta}{\varepsilon^\alpha}$; it therefore makes sense to apply the rescaling

$$\bar{w} = \varepsilon^\alpha \tilde{w} \quad \text{and} \quad \delta = \varepsilon^\alpha \tilde{\delta}$$

to Equation (3), which gives

$$\dot{\bar{v}} = -\bar{z} + f_2\bar{v}^2 + \sqrt{\varepsilon} f_3 \bar{v}^3, \tag{9a}$$

$$\dot{\bar{z}} = \bar{v} - \varepsilon^\alpha \tilde{w}, \tag{9b}$$

$$\dot{\tilde{w}} = \tilde{\delta}(\mu - \varepsilon g_1 \bar{z}). \tag{9c}$$

(In particular, it follows that $w = \varepsilon^{\frac{1}{2}+\alpha}\tilde{w}$, by the above scaling.) Under the assumption that $\tilde{\delta} = \mathcal{O}(1)$, Equation (9) exhibits delayed-Hopf-type dynamics: an orbit starting in a point $(\bar{v}, \bar{z}, \tilde{w})$, with $\tilde{w} < 0$, will take some time to become $\mathcal{O}(\tilde{\delta})$-close to $\mathcal{M}_\varepsilon$, whereby $\tilde{w}$ will only change infinitesimally. Thus, the value of $\tilde{w}$ marks the entry point of the orbit, or the 'way in'. Along $\mathcal{M}_\varepsilon$, the orbit will rotate while $\tilde{w}$ increases slowly; at the same time, the stability of $\mathcal{M}_\varepsilon$ will change, from attracting to repelling. Hence, one can define an exit point (the 'way out') for the orbit; mathematically

speaking, the former is determined such that orbits stay $\mathcal{O}(\tilde{\delta})$-close to $\mathcal{M}_\varepsilon$ as $\tilde{\delta} \to 0$ before reaching the exit point, whereas they will lie close to a fibre of the fast system corresponding to Equation (8) beyond that point. We emphasise that the exit point itself is only defined in the limit as $\tilde{\delta} \to 0$; in fact, the restriction to $\bar{w} = \Theta(\varepsilon^\alpha)$, with $0 < \alpha < \frac{1}{2}$, ensures that $\tilde{\delta}$ remains small even in the sub-scenario when $\delta = \sqrt{\varepsilon}$, considered below.

It is a classical result [12] that the relation between the entry value $\tilde{w}^{\text{in}}$ of $\tilde{w}$ and the exit value $\tilde{w}^{\text{out}}$, which is known as the 'entry-exit relation' or the 'way in-way out relation', is determined by balancing the amount of attraction and the amount of repulsion during the drift of orbits along $\mathcal{M}_\varepsilon$:

$$\int_{\tilde{w}^{\text{in}}}^{\tilde{w}^{\text{out}}} \Re\big(\lambda_\pm|_{\bar{w}=\varepsilon^\alpha \tilde{w}}\big)\, d\tilde{w} = 0, \tag{10}$$

with $\lambda_\pm$ the eigenvalues of the linearisation of Equation (8) about $\mathcal{M}_\varepsilon$, as above. Equation (10) is valid for $(\tilde{w}^{\text{in}}, \tilde{w}^{\text{out}})$ in some neighbourhood of the Hopf bifurcation point at $\tilde{w} = 0$, but loses validity at an appropriately defined 'buffer point' beyond which a different relation holds. In our case, it can be shown that this buffer point is $\Theta(\varepsilon^{-\alpha})$-bounded away from $\tilde{w} = 0$; in other words, the relation in (10) is valid for any pair $(\tilde{w}^{\text{in}}, \tilde{w}^{\text{out}})$, provided ε is sufficiently small. (The non-analyticity of (9) with respect to ε is not relevant in the present context.)

Remark 3. *While Equation* (3) *also exhibits delayed-Hopf-type dynamics, the scaled system in* (9) *has the advantage that eigenvalues of the corresponding fast subsystem have non-zero imaginary part due to our restriction of the phase space to* $\bar{w} = \Theta(\varepsilon^\alpha)$*, which facilitates the evaluation of the entry-exit relation in* (10)*. We also note that the equilibrium present in Equation* (9) *satisfies* $\tilde{w} = \Theta(\sqrt{\mu}\varepsilon^{-\frac{1}{2}-\alpha})$*. In the parameter regime considered here, with* $\mu = \mathcal{O}(\varepsilon)$*, that equilibrium hence does not play a significant role for the dynamics, whereas its effect would be pronounced in an unscaled coordinate frame.* □

Evaluating the integral in (10) explicitly and solving for balance, we find the expression $\tilde{w}^{\text{out}} = -\tilde{w}^{\text{in}}$ for the exit point when $\tilde{\delta}$ is close to 0. In terms of the original $\bar{w}$-variable, it then follows that $\bar{w}^{\text{out}} = -\bar{w}^{\text{in}}$, which implies the following leading-order approximation for the transition map Π^{dH} in the delayed-Hopf regime:

Proposition 1. *To leading order in* ε *and* δ*, the map* $\Pi^{\text{dH}} : \Delta_- \to \Delta_-$ *is given by*

$$\Pi^{\text{dH}}(w) = -w + \mathcal{O}(\delta\sqrt{\varepsilon}) \quad \text{for } w = \Theta(\varepsilon^{\frac{1}{2}+\alpha}) \tag{11}$$

with $0 < \alpha < \frac{1}{2}$*, provided* $\sqrt{\varepsilon} \in [0, \sqrt{\varepsilon_0}]$ *and* $\delta = \mathcal{O}(\varepsilon^\alpha)$*.*

Strictly speaking, the map Π^{dH} does not have Δ_- as its domain for non-zero ε; however, the error incurred by the projection onto that section which is, for simplicity, assumed in Proposition 1 is negligible to the order considered here. Finally, Π^{dH} is hence given by the negative identity – *i.e.*, by a reflection about the (v, z)-plane – to leading order. By contrast, its sector-type counterpart Π^{sec} was seen to correspond to a near-identity transformation in Section 2.2.1; recall Equation (7).

Remark 4. *We note that both sector-type SAOs and those of delayed-Hopf type share a common axis of rotation: the former oscillate (locally) about the 'weak canard'* [11] *of the singularity at the origin in Equation* (1)*; however, that canard agrees with the manifold* $\mathcal{M}_\varepsilon$ *which constitutes the axis of rotation for delayed-Hopf-type SAOs, as discussed in the present subsection.* □

3. Global dynamics

When $\delta = \varepsilon$, a geometric explanation for how Equation (1) can generate MMO dynamics was given in [9]; for future reference, we briefly restate their reasoning here. Let $\mathcal{C}_\varepsilon^-$ and $\mathcal{C}_\varepsilon^+$ be defined

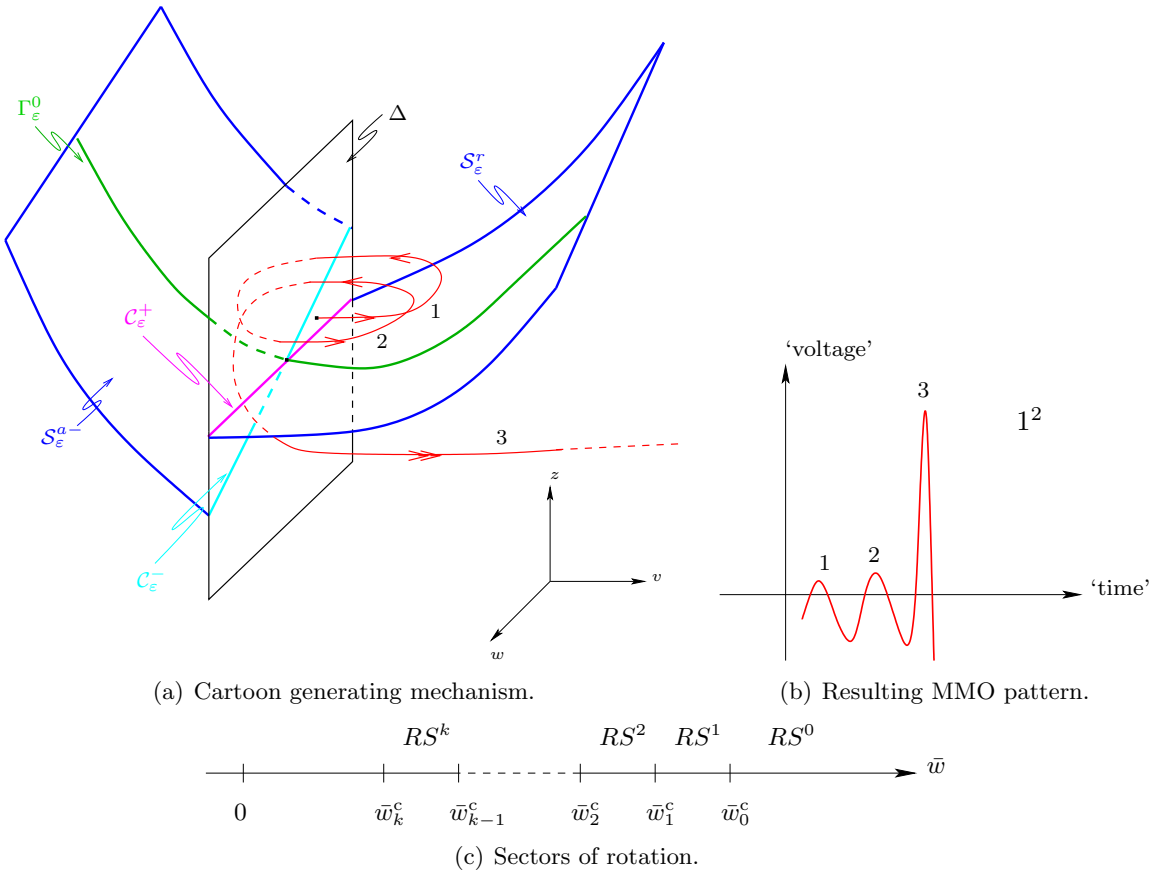

(a) Cartoon generating mechanism.

(b) Resulting MMO pattern.

(c) Sectors of rotation.

FIGURE 4. Generation of mixed-mode dynamics for $\delta = \varepsilon$ in (1). Trajectories initialised above $\mathcal{C}_\varepsilon^+$ in Δ undergo an SAO, while those below relax, as can be seen in panel 4(a); the corresponding mixed-mode pattern is shown in panel 4(b). Panel 4(c) illustrates schematically the geometry of the sectors of rotation RS^k.

as the curves of intersection of $\mathcal{S}_\varepsilon^{a-}$ and $\mathcal{S}_\varepsilon^r$, respectively, with the section Δ; see Figure 4(a). The critical w-value w_0^c at which $\mathcal{C}_\varepsilon^-$ and $\mathcal{C}_\varepsilon^+$ intersect corresponds to the strong canard Γ_ε^0, which organises the flow in a neighbourhood of ℓ^-. Trajectories starting sufficiently close to $\mathcal{S}_\varepsilon^{a-}$, but away from ℓ^-, are exponentially attracted to the former; once they reach the curve $\mathcal{C}_\varepsilon^-$, they will undergo an SAO if their w-coordinate thereon satisfies $w < w_0^c$, *i.e.*, if they lie above the curve $\mathcal{C}_\varepsilon^+$, and return to $\mathcal{S}_\varepsilon^{a-}$ near ℓ^-. If, on the other hand, they lie below $\mathcal{C}_\varepsilon^+$, with $w > w_0^c$, they will relax and leave the fold region, as illustrated schematically in Figure 4(a); the resulting mixed-mode pattern is shown in Figure 4(b). During the global return, w is reset, and the process can start anew, leading to closed MMO trajectories; in fact, it is clear from Equation (1c) that w increases in an SAO phase, whereas it decreases during relaxation. In particular, the number k of SAOs in any such trajectory then corresponds to a subinterval of the w-axis, which is called the kth sector of rotation RS^k; cf. Figure 4(c). (Hence, the trajectory undergoes relaxation once it reaches the zeroth sector of rotation, RS^0.) Finally, the boundaries between these sectors are marked by bifurcating 'secondary canards', the first of which (Γ_ε^1) is sketched in Figure 1; the reader is referred to [9] for a detailed discussion.

3.1. **Return mechanism.** While we needed to distinguish locally between the two regimes of sector behaviour and delayed-Hopf-type dynamics, the global mechanism of re-injection into the fold region after relaxation is largely regime-independent.

For simplicity, we approximate that mechanism by a map Π^{ret} which is defined on the section Δ under the additional restriction that $w > w_0^{\mathrm{c}}$; in other words, we neglect the fast ('layer') dynamics of Equation (1). Moreover, following [9, Section 2.5], we assume that Π^{ret} returns trajectories to the fold line ℓ^-, instead of to some neighbourhood thereof, *i.e.*, we interpret Π^{ret} as a map from ℓ^- to itself. (The exponential contraction towards $\mathcal{S}_0^{a\pm}$, to leading order, ensures that the image of any point in Δ under Π^{ret} will, in fact, lie $\mathcal{O}(\varepsilon)$-close to ℓ^-.)

Lemma 2. *To leading order in ε and δ, the map $\Pi^{\mathrm{ret}} : \Delta \to \Delta$ is given by*

$$\begin{aligned} \Pi^{\mathrm{ret}}(w) &\sim w + \delta\big[\mathcal{G}(v_0, v_{\max}, \mu) + \mathcal{G}(v_{\max}^*, 0, \mu)\big] \\ &= w + \delta\left(\frac{g_1}{18}\frac{f_2^5}{f_3^3} - \mu\frac{f_2^2}{f_3}\right) \end{aligned} \tag{12}$$

for $w > w_0^{\mathrm{c}}$. (Here, $\mathcal{G}(v_-, v_+, \mu) = \int_{v_-}^{v_+}[\mu - g_1 f(\sigma)]\frac{f'(\sigma)}{\sigma}\,d\sigma$.)

Proof. As in [9], we consider the projection of the reduced flow corresponding to Equation (1) onto the critical manifold $\mathcal{S}_0$: noting that $z = f(v)$ implies $\dot{z} = f'(v)\dot{v}$ and desingularising the resulting flow by multiplication with a factor of $-f'(v)$, which is positive on the attracting portion $\mathcal{S}_0^{a\pm}$ of $\mathcal{S}_0$, we find

$$\begin{aligned} \dot{v} &= -v + w, \\ \dot{w} &= -\delta f'(v)[\mu - g_1 f(v)]. \end{aligned}$$

Since $w = \mathcal{O}(1)$, by assumption, we may write $\frac{dw}{dv} \sim \delta\frac{f'(v)}{v}[\mu - g_1 f(v)]$, which we integrate to obtain the leading-order approximation for the global return of trajectories from Δ to itself under the singular flow of (1):

$$\begin{aligned} \Pi^{\mathrm{ret}}(w) &\sim w + \delta\left\{\int_{v_0}^{v_{\max}}[\mu - g_1 f(\sigma)]\frac{f'(\sigma)}{\sigma}\,d\sigma + \int_{v_{\max}^*}^{0}[\mu - g_1 f(\sigma)]\frac{f'(\sigma)}{\sigma}\,d\sigma\right\} \\ &\equiv w + \delta\big[\mathcal{G}(v_0, v_{\max}, \mu) + \mathcal{G}(v_{\max}^*, 0, \mu)\big]. \end{aligned}$$

Here, $v_{\max}$ is the v-value at which the function f assumes its local maximum, v_0 denotes the rightmost zero of f, and $v_{\max}^* \neq v_{\max}$ is defined by the requirement that $f(v_{\max}^*) = f(v_{\max})$; see Figure 5 for an illustration. Evaluation of the above expression gives Equation (12), as claimed. □

We emphasise that the distance between the 'jump-off' point $w \in \Delta$ and the point $\Pi^{\mathrm{ret}}(w)$ of re-entry into the fold region only depends on δ and μ, to the order considered here, as well as that Equation (12) is equivalent to [9, Equation (2.54)], with ε there replaced with δ here. Finally, we note that the critical μ-value μ^{c} beyond which pure relaxation dynamics is observed is δ-independent, as it is found by solving $\mathcal{G}(v_0, v_{\max}, \mu) + \mathcal{G}(v_{\max}^*, 0, \mu) = 0$ for μ: $\mu^{\mathrm{c}} = \frac{g_1}{18}\frac{f_2^3}{f_3^2}$; cf. [9, Equation (2.56)].

3.2. **Reduced Poincaré map.** In this subsection, we indicate how a reduced (one-dimensional) Poincaré map can be constructed for Equation (1). As in [9], that map will be a function of w or, equivalently, of its rescaled counterpart $\bar{w}$, and will incorporate both the local dynamics of (1) in a neighbourhood of the origin in (v, z, w)-space and the global flow on the slow manifold – or rather, on the two attracting sheets $\mathcal{S}_\varepsilon^{a\pm}$ thereof – away from $(v, z, w) = (0, 0, 0)$.

We discuss the sector regime first, recalling that the analysis in [9] was restricted to the case where the number of SAOs is not 'too large' – in the single digits, practically speaking – as the asymptotics

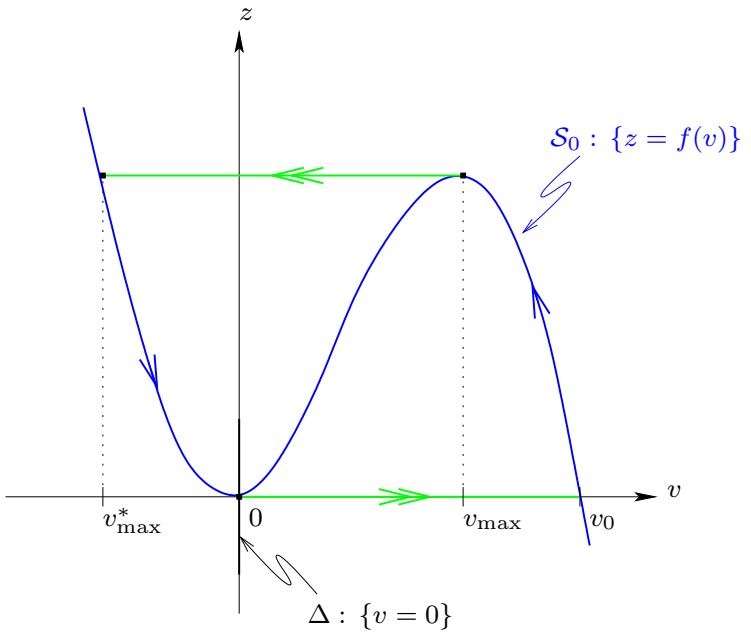

FIGURE 5. Global return mechanism for (1). The map Π^{ret} is approximated by the reduced dynamics on $\mathcal{S}_0$ to the order considered here, whereas the layer flow is neglected.

may become inconsistent otherwise, leading to an accumulation of error. (Consequently, one has to assume that any initial values for Equation (1) are sufficiently close to the strong canard Γ^0_ε in that regime. As we will initialise the flow of (1) in the section Δ throughout the following discussion, that assumption translates to closeness to the origin initially.) Under the above restriction, the reduced return map $\Pi : \Delta \to \Delta$ is, in essence, described by the local map Π^{sec}, Equation (7), whenever $w < w_0^{\text{c}}$ with $w = \Theta(\varepsilon)$ for the corresponding trajectory, *i.e.*, whenever that trajectory undergoes another SAO; cf. Section 2.2.1. Similarly, it is to a first approximation given by the global return Π^{ret}, Equation (12), if $w > w_0^{\text{c}}$, that is, once the trajectory leaves the fold region to undergo relaxation. (A simplification is achieved by neglecting the repulsion from Δ pre-relaxation, as well as the attraction towards Δ post-relaxation, *i.e.*, after the trajectory has returned to the fold region, which were labelled the 'entry' and 'exit' maps, respectively, in [9].)

If, on the other hand, the trajectory is far enough from the origin initially (in Δ) to be attracted to the ε-family of critical manifolds $\mathcal{M}_\varepsilon$, *i.e.*, if $w < w_0^{\text{c}}$ with $w = \Theta(\varepsilon^{\frac{1}{2}+\alpha})$ for some $0 < \alpha < \frac{1}{2}$, the delayed-Hopf regime is realised locally. In that case, results from [12] can be applied to approximate the return map for Equation (1). In particular, the local component of that map will be defined as in Equation (11), recall Section 2.2.2, whereas the global return will still be described by Equation (12). (For simplicity, we consider neither the fast repulsion from $\mathcal{M}_\varepsilon$ pre-relaxation, nor the fast attraction towards $\mathcal{M}_\varepsilon$ post-relaxation here.)

The question remains of how to distinguish between the two regimes; in other words, we need to determine some critical initial w-value w^* which separates sector-type dynamics from delayed-Hopf-type behaviour. (While Lemma 1 and Proposition 1 approximate the return from the section Δ_- to itself in the two regimes, with $w = \Theta(\varepsilon)$ and $w = \Theta(\varepsilon^{\frac{1}{2}+\alpha})$, respectively, the transition between the former and the latter was not considered in Section 2.2.) Specifically, let w^* be defined such that, if $w_0 > w^*$ initially in Δ, the corresponding trajectory is repelled away from the attracting

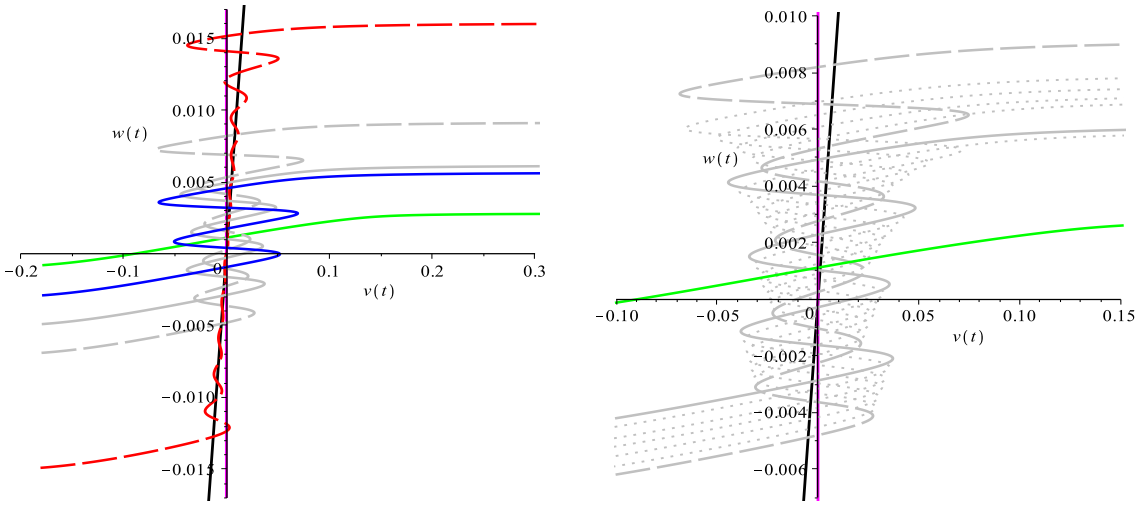

(a) Representative orbits in (v, w)-plane.

(b) Zoom onto origin.

FIGURE 6. Transition between sector-type and delayed-Hopf-type dynamics for $\delta = \sqrt{\varepsilon}$ in (1) ($\varepsilon = 0.01$, $\delta = 0.1$, $\mu = 0.04$). The corresponding critical w-value w^* in panel 6(a) may be estimated via a numerical sweep of initial values w_0; cf. panel 6(b). For reference, the strong canard Γ_ε^0 (solid green), the fold line ℓ^- (solid purple), and the manifold $\mathcal{M}_\varepsilon$ (solid black) are superimposed.

slow manifold $\mathcal{S}_\varepsilon^{a-}$ as soon as it satisfies $w > w_0^c$, *i.e.*, once it reaches the zeroth sector of rotation, RS^0.

For illustration, let us consider the example presented in Figure 6, with $\varepsilon = 0.01$, $\delta = 0.1$, and $\mu = 0.04$. In Figure 6(a), several orbits with initial conditions close to $\mathcal{S}_\varepsilon^{a-}$ are shown. The dashed red orbit is a realisation of the delayed-Hopf mechanism: it is near-symmetric about the origin and incorporates a substantial number of SAOs which first decrease and then increase in amplitude. (In particular, the attracting character of the ε-family of critical manifolds $\mathcal{M}_\varepsilon$ is evident from the figure.) The solid blue orbit, on the other hand, realises the sector mechanism, whereby a small number of SAOs of moderate and increasing amplitude is observed. Experimenting with initial w-values that lie between those corresponding to these two orbits, one can estimate w^* numerically: thus, the solid grey orbit in Figure 6 is still of sector type; moreover, the w-value at which it jumps off S_ε^{a-} is almost equal to that found for the blue orbit. By contrast, the dashed grey orbit, obtained by increasing $|w_0|$ further, undergoes an additional SAO in RS^0. A numerical sweep of w_0-values (dotted grey) in between those corresponding to the solid and dashed grey orbits reveals that the latter yields the highest initial value for which such an SAO occurs; see Figure 6(b). Hence, it follows that $w^* \approx -0.005$, which is consistent with the above scaling regimes.

4. Sector-delayed-Hopf-type dynamics

The construction performed in Section 3.2 can aid in elucidating the mechanism whereby trajectories of Equation (1) display mixed sector-delayed-Hopf-type behaviour. We are not aware of previous reports of such patterns in the published literature, and hence believe them to represent a novel class of complex oscillatory dynamics in singularly perturbed fast-slow systems of the type in Equation (1).

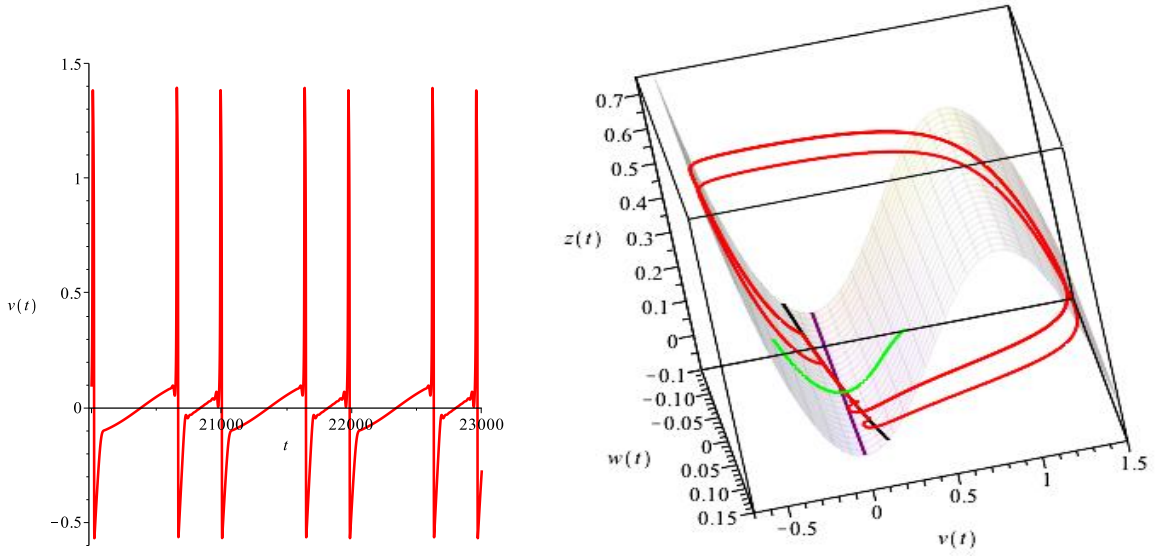

(a) Time series of v.

(b) Orbit in (v, z, w)-space.

FIGURE 7. Delayed-Hopf-type MMO dynamics for $\delta = \sqrt{\varepsilon}$ in (1) ($1^{d_1}1^{d_2}$; $\varepsilon = 0.05$, $\delta = 0.4$, $\mu = 0.02$). For reference, the strong canard Γ_ε^0 (solid green), the fold line ℓ^- (solid purple), the manifold $\mathcal{M}_\varepsilon$ (solid black), and the critical manifold $\mathcal{S}_0$ (shaded) are included in panel 7(b).

As discussed towards the beginning of Section 2, stable mixed-mode dynamics will be observed for $\delta = \varepsilon$ in (1), provided the flow remains sufficiently close to the strong canard Γ_ε^0 in (v, z, w)-space. However, trajectories that are initialised far away from the origin in Δ – with $w_0 < w^*$, in the notation of the previous section – will be attracted to the one-dimensional ε-family of critical manifolds $\mathcal{M}_\varepsilon$ of the 'zoomed' system, Equation (3), instead. The flow thus bypasses the fold region entirely in such cases before being repelled away from $\mathcal{M}_\varepsilon$, in accordance with a delayed-Hopf mechanism. Furthermore, the value of w attained at that point will no longer correspond to a sector of rotation; in particular, orbits will not necessarily relax once they reach RS^0, as was already evident in Figure 6. Finally, since Equation (12) implies that the strength of the global return mechanism in (1) increases with δ, *i.e.*, that $\frac{\partial \Pi^{\mathrm{ret}}}{\partial \delta} = \mathcal{G}_1 + \mathcal{G}_2 < 0$ for $\mu < \mu^{\mathrm{c}}$, $\Pi^{\mathrm{ret}}(w) < w^*$ may again hold after relaxation; hence, the flow may return to $\mathcal{M}_\varepsilon$. In other words, the return point will no longer necessarily be close to the strong canard, as was the case in Section 2.2.1 [9]; rather, it will correspond to the 'way in' for the delayed-Hopf-type dynamics discussed in Section 2.2.2, in accordance with Equation (10). In fact, the larger $|w_0 - w^*|$ is, the stronger the attraction to $\mathcal{M}_\varepsilon$ during a delayed-Hopf-type segment, leading to an increase in the duration of that segment. Correspondingly, Equation (1) may display stable MMO-type dynamics for $\delta > \varepsilon$ in which SAOs are based on the delayed-Hopf phenomenon; see Figure 7 for an example, where we chose $\varepsilon = 0.05$, $\delta = 0.4$, $\mu = 0.02$, and $(v_0, z_0, w_0) = (0, 0, -0.01)$.

Much more unexpected is the fact that we have also found periodic solution trajectories in which both sector-type and delayed-Hopf-type segments are present. Such behaviour can be observed if the flow is alternately re-injected close to the strong canard and far away from it, leading to patterns in which sector-type SAOs alternate with those of delayed-Hopf type.

We have tested the above conceptual argument numerically, as illustrated in Figures 8 through 10. (Throughout, we take $\varepsilon = 0.01$, $\delta = 0.1$, and $\mu = 0.04$, as before; moreover, we assume that

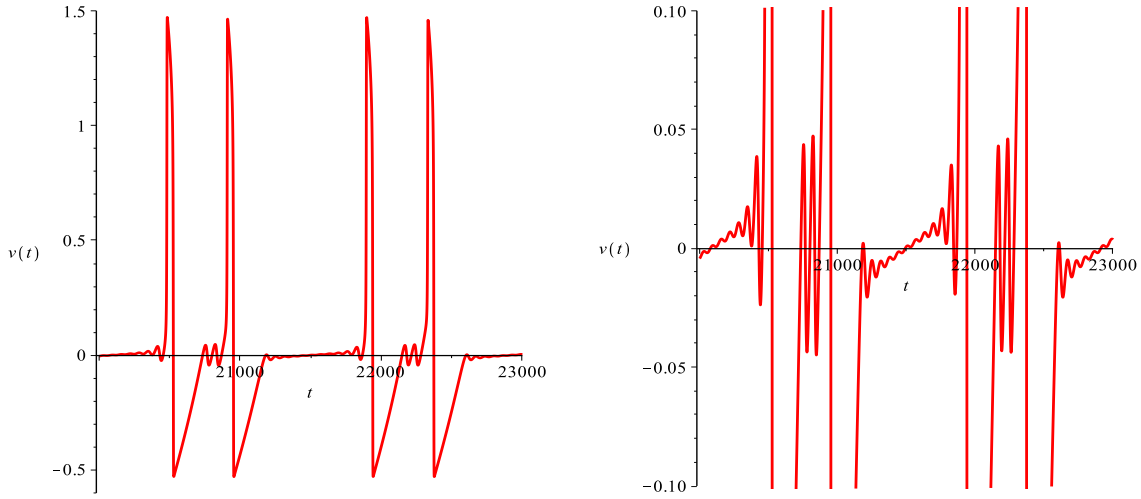

(a) Time series of v.

(b) Zoom onto SAO component.

FIGURE 8. Mixed sector-delayed-Hopf-type dynamics for $\delta = \sqrt{\varepsilon}$ in (1) ($1^2 1^d$; $\varepsilon = 0.01$, $\delta = 0.1$, $\mu = 0.04$).

$(v_0, z_0) = (0, 0)$, *i.e.*, that the initial conditions for Equation (1) are chosen in Δ, as indicated previously.) Figure 8 shows a periodic pattern with signature $1^2 1^d$, where the initial condition was taken as $w_0 = -0.01$: we observe delayed passage through a Hopf bifurcation followed by relaxation, two sector-type SAOs in sequence, and then again relaxation, at which point the process repeats periodically; cf. Figure 8(a). The signature of the delayed-Hopf-type segment in the time series becomes visible after a zoom onto its SAO component, giving $d = 11$; see Figure 8(b). Similarly, in Figure 9, a periodic $1^3 1^d$-type pattern is presented, with initial condition $w_0 = -0.00845$; finally, in Figure 10, we observe a periodic pattern with signature $1^4 1^d$, where we chose $w_0 = -0.00723$ initially.

A leading-order approximation for the reduced return map corresponding to mixed sector-delayed-Hopf-type trajectories with Farey signature $1^k 1^d$ can be defined as follows: $w_0 \mapsto \Pi(w_0) := \big(\Pi^{\mathrm{ret}} \circ \Pi^{\mathrm{dH}} \circ \Pi^{\mathrm{ret}} \circ (\Pi^{\mathrm{sec}})^k\big)(w_0)$, for some $k \in \mathbb{N}$. Concatenating the asymptotics of Π^{sec}, Π^{dH}, and Π^{ret}, as given in Equations (7), (11), and (12), we thus have

$$\Pi(w_0) \sim -w_0 + 2\delta\left(\frac{g_1}{18}\frac{f_2^5}{f_3^3} - \mu\frac{f_2^2}{f_3} + k\sqrt{2}\mu\sqrt{\varepsilon}\sqrt{-\ln\varepsilon}\right), \tag{13}$$

to leading order in ε and δ.

Evaluating Equation (13) for $k = 2$, 3, and 4 – *i.e.*, in the three parameter regimes illustrated in Figures 8 through 10 – we find that throughout, the discrepancy between w_0 and $\Pi(w_0)$ is well within the $\mathcal{O}(\delta\sqrt{\varepsilon})$-error predicted analytically. Correspondingly, the phase portraits shown in Figures 9(b) and 10(b) confirm visually that the orbits obtained for the above (empirical) choices of w_0 are periodic.

5. Discussion

In the present article, we have considered a modification of a three-time-scale system that was proposed in [9] as a canonical model for 'slow passage through a classical canard explosion'. We have shown that, by changing the hierarchy of scales therein to a sufficient degree, we can construct orbits which contain segments of both sector type and delayed-Hopf type; while the former are generated

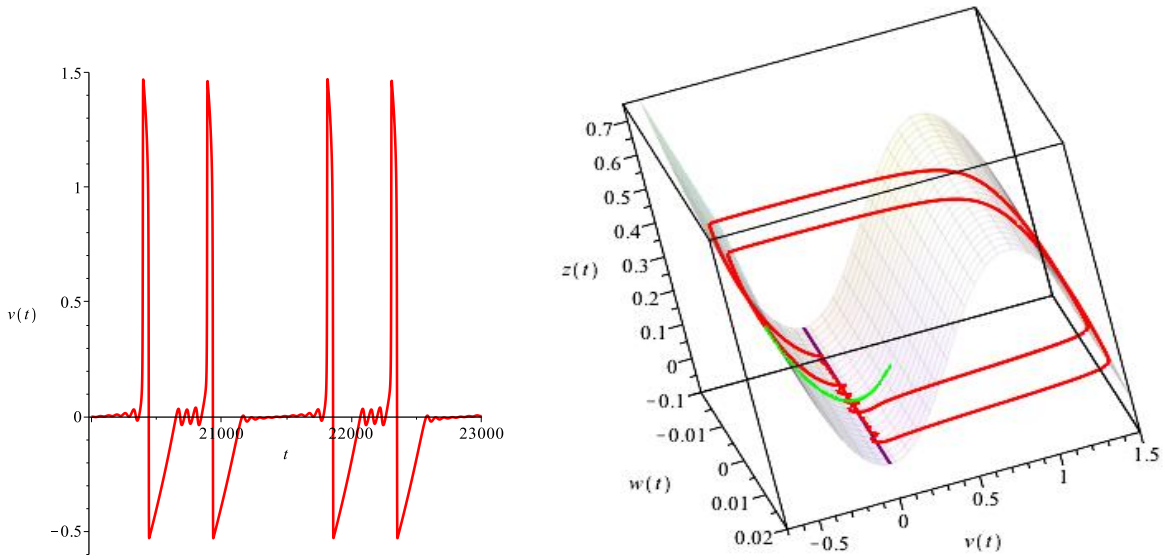

(a) Time series of v.

(b) Orbit in (v, z, w)-space.

FIGURE 9. Mixed sector-delayed-Hopf-type dynamics for $\delta = \sqrt{\varepsilon}$ in (1) ($1^3 1^d$; $\varepsilon = 0.01$, $\delta = 0.1$, $\mu = 0.04$). For reference, the strong canard Γ_ε^0 (solid green), the fold line ℓ^- (solid purple), and the critical manifold $\mathcal{S}_0$ (shaded) are included in panel 9(b).

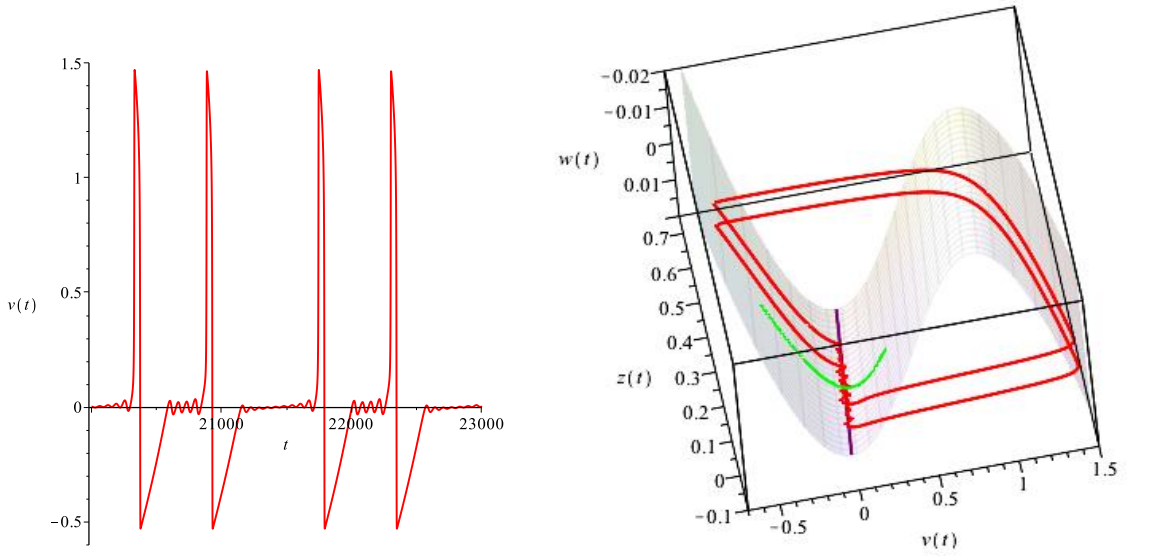

(a) Time series of v.

(b) Orbit in (v, z, w)-space.

FIGURE 10. Mixed sector-delayed-Hopf-type dynamics for $\delta = \sqrt{\varepsilon}$ in (1) ($1^4 1^d$; $\varepsilon = 0.01$, $\delta = 0.1$, $\mu = 0.04$). For reference, the strong canard Γ_ε^0 (solid green), the fold line ℓ^- (solid purple), and the critical manifold $\mathcal{S}_0$ (shaded) are included in panel 10(b).

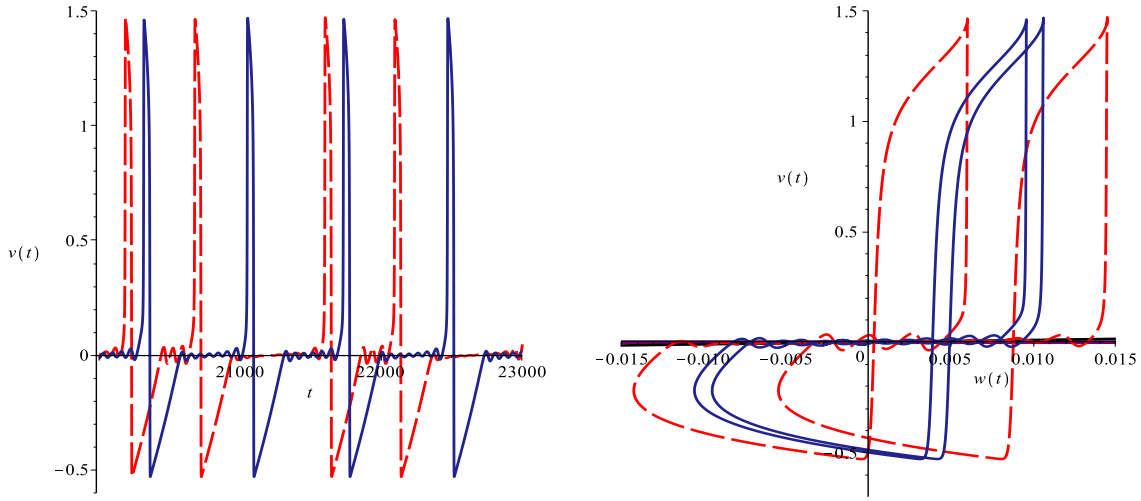

(a) Time series of v.

(b) Orbit in (v, w)-plane.

FIGURE 11. Mixed sector-delayed-Hopf-type dynamics for $\delta = \sqrt{\varepsilon}$ in (1) (dashed red: $1^3 1^{10}$, $\mu = 0.04$; solid blue: $1^6 1^7$, $\mu = 0.0399$; $\varepsilon = 0.01$, $\delta = 0.1$). For reference, the fold line ℓ^- (solid purple) and the manifold $\mathcal{M}_\varepsilon$ (solid black) are included in panel 11(b).

by a local passage through a neighbourhood of a folded saddle-node of type II in Equation (1), the latter arise from a dynamic Hopf bifurcation along an appropriately defined ε-family of critical manifolds thereof. Furthermore, we have adapted the construction of the reduced (one-dimensional) Poincaré map presented in [9, Section 3] to incorporate delayed-Hopf-type dynamics. A general reduction of the *a priori* two-dimensional Poincaré map for Equation (1) to one dimension seems to be a challenging task; however, following [9] and [12] and making a number of simplifying assumptions, we have achieved an asymptotic approximation which seems to be sufficiently accurate for our purposes, as evidenced in Section 4. That approximation, Equation (13), reflects the delicate interplay between local and global aspects of the flow of Equation (1) in generating sector-delayed-Hopf-type mixed-mode dynamics therein.

In the process, a number of qualitative differences have emerged between the scenario considered in [9], with $\delta = \varepsilon$ in Equation (1), and the one studied here, where $\delta > \varepsilon$ is assumed. In particular, the periodic mixed-mode patterns that were observed in the original model are not generic anymore in our case; rather, they tend to occur in isolation. An example is provided in Figure 11, where an $\mathcal{O}(\varepsilon^2)$-decrease in μ – from $\mu = 0.04$ to $\mu = 0.0399$ – results in a transition between the signatures $1^3 1^{10}$ and $1^6 1^7$. (Here, we have specified the number of Hopf-type SAOs for ease of comparison, in contrast to our usual practice of leaving it unspecified, as d.)

Moreover, we emphasise that, while the mixed sector-delayed-Hopf-type patterns described in Section 4 appear periodic and stable, they do not seem to be globally stable: the signatures $1^3 1^d$ and $1^4 1^d$, for instance, are obtained for identical values of ε, δ, and μ, but different values of w_0, and must hence possess disjoint basins of attraction (in w); recall Figures 9 and 10. Preliminary numerical results suggest a complicated topology of these basins, as patterns with given signature $1^k 1^d$ do not seem to correspond to connected w_0-intervals but, rather, to unions of such intervals. (Roughly speaking, the latter seem to be interleaved with the basins of attraction of 'adjacent' patterns with signatures $1^{k-1} 1^d$ and $1^{k+1} 1^d$.) By contrast, the 'pure' MMO patterns that were described in [9] for

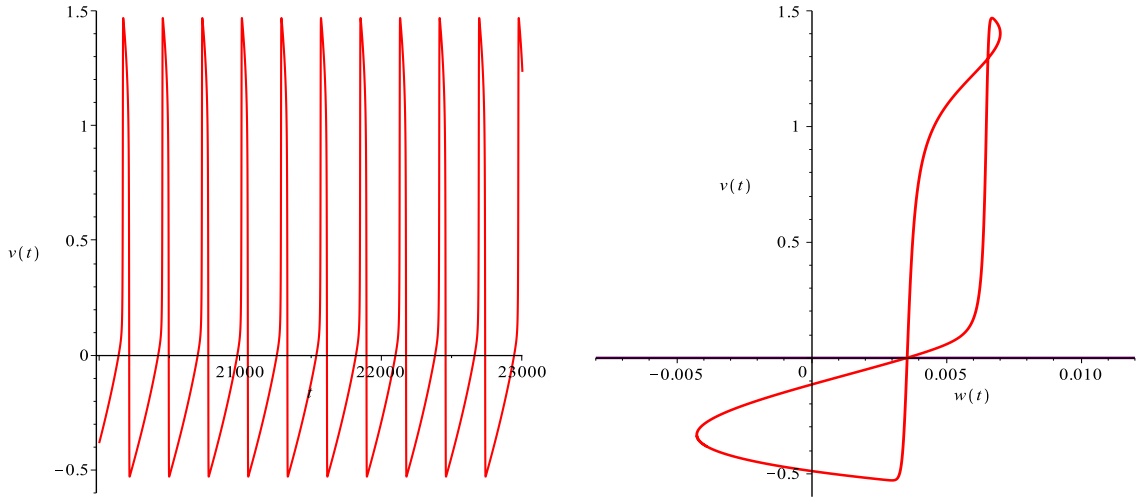

(a) Time series of v.

(b) Orbit in (v, w)-plane.

FIGURE 12. Relaxation-type dynamics for $\delta = \sqrt{\varepsilon}$ in (1) (1^0; $\varepsilon = 0.01$, $\delta = 0.1$, $\mu = 0.1$). For reference, the fold line ℓ^- (solid purple) is included in panel 12(b).

$\delta = \varepsilon$ in Equation (1) were globally stable. Overall, the dynamics of the generalised Equation (1) thus seems less robust when $\delta > \varepsilon$, as compared to the scenario considered in [9].

However, we have also identified a number of similarities between the two scenarios. Thus, the onset of relaxation oscillation will coincide, at least to leading order, since the critical μ-value μ^c is independent of both ε and δ, as can be seen in Figure 12. (Here, $\mu = 0.1$ is chosen larger than, but close to, $\mu^c \approx 0.09375$.) Hence, the dynamics of Equation (1) will be similar to that found in [9] whenever $|\mu - \mu^c|$ is small: the return will be close to the strong canard Γ^0_ε, recall Section 3, resulting in MMO-like patterns with a low number of SAOs; examples can be seen in Figures 13 ($\mu = 0.08$) and 14 ($\mu = 0.075$). (Intuitively speaking, the $\mathcal{G}$-dependent term in Equation (12) can compensate for an increase in δ for sufficiently small $|\mu - \mu^c|$.) For larger values of μ, the global return mechanism will ultimately push w below its critical value w^*, thus ruining the regular Farey-like bifurcation structure that was observed in [9].

Correspondingly, the transition between sector dynamics and delayed-Hopf-type behaviour in Equation (1) is not 'hard': the two types of dynamics may, in fact, be interpreted as extreme realisations of the same mechanism. The separation between those will, in reality, not be abrupt, as is suggested by our definition of the critical w-value w^*; in other words, an intermediate regime will exist in which orbits will gradually transition between the two extremes, as can be seen from the 1^61^7-type pattern in Figure 11, for instance. Finally, as $\delta \to \varepsilon$, one should observe a regular transition to the sector regime considered in [9]: in fact, even in the scenario considered there, orbits appear increasingly 'Hopf-like' with increasing number of SAOs, in the sense that a decrease in amplitude is followed by a corresponding increase before relaxation.

Our discussion of the mixed sector-delayed-Hopf-type dynamics that is observed numerically for $\delta = \Theta(\sqrt{\varepsilon})$ in Equation (1) has been largely informal. We have constructed an approximate reduced Poincaré map in that scenario; however, we have neglected the entry into, and the exit from, a neighbourhood of the origin in phase space in our analysis. While the resulting approximation seems reasonable in some parameter regimes, as was seen in Section 4, it may fail in others. Thus, our reduced map will not apply in an intermediate regime – with w close to its critical value w^* – in which the number of SAOs in the trajectory is too large to allow for an application of the

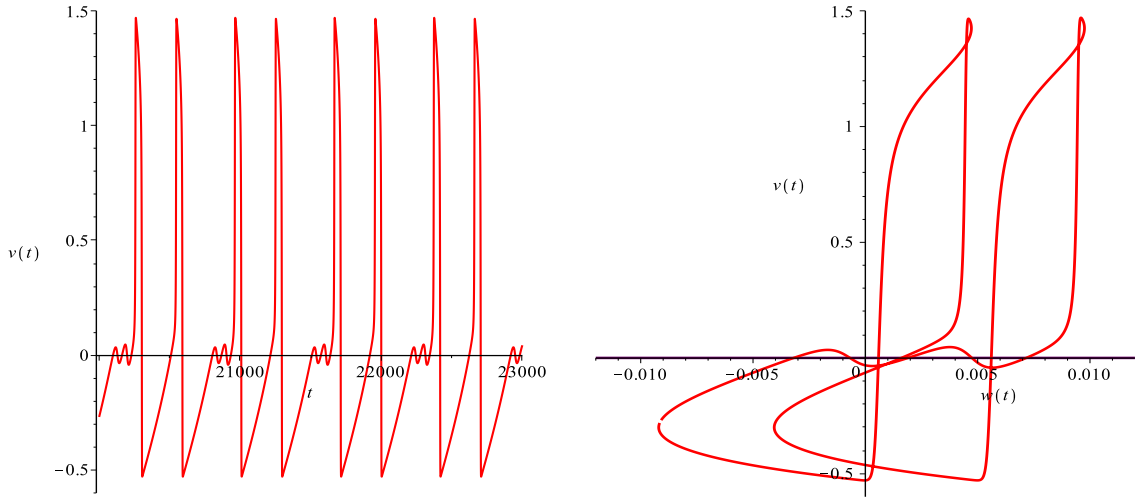

(a) Time series of v.

(b) Orbit in (v, w)-plane.

FIGURE 13. Sector-type MMO dynamics for $\delta = \sqrt{\varepsilon}$ in (1) (2^2; $\varepsilon = 0.01$, $\delta = 0.1$, $\mu = 0.08$). For reference, the fold line ℓ^- (solid purple) is included in panel 13(b).

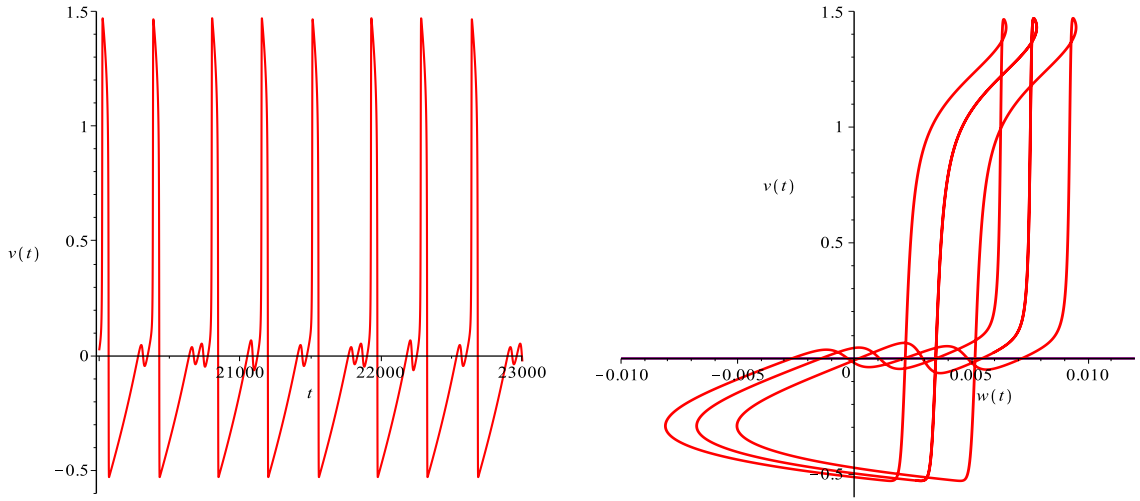

(a) Time series of v.

(b) Orbit in (v, w)-plane.

FIGURE 14. Sector-type MMO dynamics for $\delta = \sqrt{\varepsilon}$ in (1) ($(1^1)^2 1^2$; $\varepsilon = 0.01$, $\delta = 0.1$, $\mu = 0.075$). For reference, the fold line ℓ^- (solid purple) is included in panel 14(b).

results obtained in [9], while the structure required by the delayed Hopf bifurcation is not fully present yet. A rigorous treatment of Equation (1) with $\delta > \varepsilon$ seems indispensable if some of the more quantitative insights from [9] are to be reproduced in the present context; two examples concern estimates for the relevant parameter intervals and the study of the stability properties of the resulting reduced Poincaré map, both of which were crucial to elucidating the unfolding of the complex bifurcation structure of Equation (1) in [9].

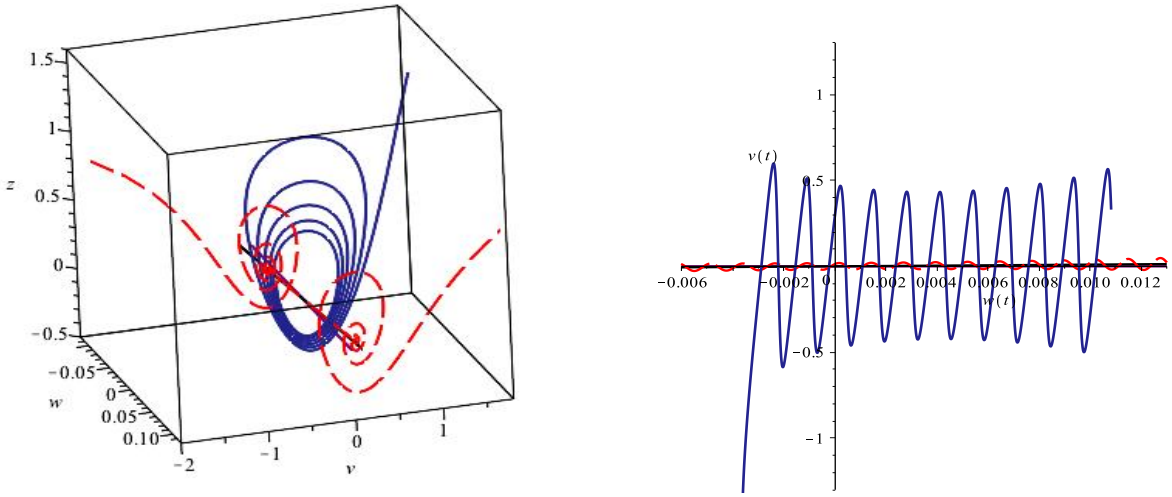

(a) Phase space geometry.

(b) Zoom onto SAO component.

FIGURE 15. Mixed-sector-delayed-Hopf-type dynamics for $\delta = \varepsilon$ in (1). Panel 15(b) indicates agreement between the frequencies of the SAOs of sector type and delayed-Hopf type shown in panel 15(a). For reference, the fold line ℓ^- (solid purple) and the manifold $\mathcal{M}_\varepsilon$ (solid black) are superimposed.

We end our discussion with several preliminary observations to that effect: our approximation for the map Π^{sec} in the sector regime, Equation (7), implies

$$\Delta w \sim -2\sqrt{2}\mu\delta\sqrt{\varepsilon}\sqrt{-\ln\varepsilon} \tag{14}$$

for the width of the k-th sector of rotation RS^k, at least to leading order in ε and for sufficiently low values of k; cf. [9, Proposition 3.3]. However, Δw also seems to give a good estimate for the frequency of delayed-Hopf-type oscillations in the 'mixed-type' trajectories described in this article; see Figure 15 for an example, with $\varepsilon = 0.01 = \delta$ and $\mu = 0.02$: Figure 15(b) confirms that the frequency of the sector-type SAO shown in Figure 15(a) (solid blue) agrees with that of the corresponding delayed-Hopf-type SAO (dashed red) in that parameter regime. (Here, the initial w-value w_0 is chosen sufficiently close to the origin for the attraction to the ε-family of critical manifolds $\mathcal{M}_\varepsilon$ not to be too strong, which makes it possible to discern small oscillations in the delayed-Hopf regime.)

Remark 5. *The estimate in Equation* (14) *can be viewed as a refinement of the corresponding, well-known result that was obtained in* [2]*, in the context of the folded node: there, the width of* RS^k *was shown to be of the order* $\Theta(\varepsilon^{\frac{1-\psi}{2}})$*, with* ψ *denoting the ratio of the weak to the strong eigenvalue of the linearisation of the desingularised reduced flow about a folded node. (We note that, in Equation* (1)*, one has* $\psi = \Theta(\delta)$*.)* □

One obstacle to a rigorous treatment of Equation (1) is the lack of analytical estimates for the critical w-value w^* which marks the transition between sector-type and delayed-Hopf-type behaviour. To that end, a refined approximation seems to be required for w_0^{c}, the value of w corresponding to the strong canard Γ_ε^0 in (1); recall Figure 1. Thus, the first-order asymptotics quoted in [9, Equation (2.16)] would imply $w_0^{\text{c}} \sim -\frac{3}{8}\frac{f_3}{f_2^3}\varepsilon \approx 0.0011$ for $\varepsilon = 0.01$, which is of the same order as the corresponding $\mathcal{O}(\varepsilon\sqrt{\varepsilon})$-error term. However, when $\delta = \sqrt{\varepsilon}$, additional contributions

will result in the expansion for w_0^c: while the near-integrable structure of Equation (3) will persist, the approximate solution $\bar{w} \sim \bar{w}_0 + \sqrt{\varepsilon}\mu t$ to Equation (3c) will now be comparable in order to the first-order correction – *i.e.*, to the $\sqrt{\varepsilon} f_3 \bar{v}^3$-term – in (3a). The resulting contributions can be derived as in [9, Section 3.3], where the near-integrability of Equation (3) is exploited to approximate the return map Π via a Melnikov-type calculation which relies on successive derivatives of the constant of motion H defined in Section 2.2.1. That same approach may lead to an improved quantitative picture of the sector geometry in the scenario considered here.

In sum, there hence seems to be the prospect of adapting some of the results obtained in [9] towards a more complete, analytical understanding of the mixed-sector-delayed-Hopf-type dynamics observed in Equation (1).

References

[1] E. Benoît, *Bifurcation delay – the case of the sequence: stable focus – unstable focus – unstable node*, Discret. Contin. Dyn. S. Series S **2**(4), 911–929, 2009.

[2] M. Brøns, M. Krupa, and M. Wechselberger, *Mixed mode oscillations due to the generalized canard phenomenon*, in Bifurcation theory and spatio-temporal pattern formation, Fields Inst. Commun. **49**, 39–63, Amer. Math. Soc., Providence, RI, 2006.

[3] M. Desroches, J. Guckenheimer, B. Krauskopf, C. Kuehn, H. Osinga, and M. Wechselberger, *Mixed-mode oscillations with multiple time scales*, SIAM Rev. **54**(2), 211–288, 2012.

[4] N. Fenichel, *Geometric singular perturbation theory for ordinary differential equations*, J. Differential Equations **31**(1), 53–98, 1979.

[5] E. Harvey, V. Kirk, M. Wechselberger, and J. Sneyd, *Multiple timescales, mixed mode oscillations and canards in models of intracellular calcium dynamics*, J. Nonlinear Sci. **21**(5), 639–683, 2011.

[6] C. K. R. T. Jones, *Geometric singular perturbation theory*, in Dynamical systems (Montecatini Terme, 1994), Lecture Notes in Math. **1609**, 44–118, Springer-Verlag, Berlin, 1995.

[7] M. Krupa, N. Popović, N. Kopell, and H. G. Rotstein, *Mixed-mode oscillations in a three time-scale model for the dopaminergic neuron*, Chaos **18**, 015106, 2008.

[8] I. Kosiuk and P. Szmolyan, *Scaling in singular perturbation problems: blowing up a relaxation oscillator*, SIAM J. Appl. Dyn. Syst. **10**(4), 1307–1343, 2011.

[9] M. Krupa, N. Popović, and N. Kopell, *Mixed-mode oscillations in three time-scale systems–a prototypical example*, SIAM J. Appl. Dyn. Syst. **7**(2), 361–420, 2008.

[10] M. Krupa and P. Szmolyan, *Relaxation oscillation and canard explosion*, J. Differential Equations **174**(2), 312–368, 2001.

[11] M. Krupa and M. Wechselberger, *Local analysis near a folded saddle-node singularity*, J. Differential Equations **248**(12), 2841–2888, 2010.

[12] A. I. Neĭshtadt, *Prolongation of the loss of stability in the case of dynamic bifurcations. I.*, Differential Equations **23**(12), 1385–1391, 1987.

[13] L. Segel and A. Goldbeter, *Scaling in biochemical kinetics: dissection of a relaxation oscillator*, J. Math. Biol. **32**(2), 147–160, 1994.

Hasselt University, Campus Diepenbeek, Agoralaan Gebouw D, B-3590 Diepenbeek, Belgium
E-mail address: Peter.DeMaesschalck@uhasselt.be

AGH University of Science and Technology, al. Mickiewicza 30, 30-059 Kraków, Poland, and Uniklinik RWTH Aachen, Department of Medical Informatics, Pauwelsstrasse 30, 52057 Aachen, Germany
E-mail address: Ekaterina.Kutafina@gmail.com

University of Edinburgh, School of Mathematics and Maxwell Institute for Mathematical Sciences, James Clerk Maxwell Building, King's Buildings, Peter Guthrie Tait Road, Edinburgh EH9 3FD, United Kingdom
E-mail address: Nikola.Popovic@ed.ac.uk